Bias in bonding behavior among boron, carbon, and nitrogen atoms in ion implanted a-BN, a-BC, and diamond like carbon films

Mustafa Fatih Genisel, Md. Nizam Uddin, Zafer Say, Mustafa Kulakci, Rasit Turan, Oguz Gulseren, and Erman Bengu

Citation: Journal of Applied Physics **110**, 074906 (2011);
View online: https://doi.org/10.1063/1.3638129
View Table of Contents: http://aip.scitation.org/toc/jap/110/7
Published by the American Institute of Physics

Bias in bonding behavior among boron, carbon, and nitrogen atoms in ion implanted *a*-BN, *a*-BC, and diamond like carbon films

Mustafa Fatih Genisel,[1] Md. Nizam Uddin,[1,a)] Zafer Say,[1] Mustafa Kulakci,[2] Rasit Turan,[2] Oguz Gulseren,[3] and Erman Bengu[1,a)]
[1]*Department of Chemistry, Bilkent University, Ankara, 06800, Turkey*
[2]*Department of Physics, Middle East Technical University, Ankara, 06531, Turkey*
[3]*Department of Physics, Bilkent University, Ankara, 06800, Turkey*

(Received 12 April 2011; accepted 8 August 2011; published online 13 October 2011)

In this study, we implanted N^+ and N_2^+ ions into sputter deposited amorphous boron carbide (*a*-BC) and diamond like carbon (DLC) thin films in an effort to understand the chemical bonding involved and investigate possible phase separation routes in boron carbon nitride (BCN) films. In addition, we investigated the effect of implanted C^+ ions in sputter deposited amorphous boron nitride (*a*-BN) films. Implanted ion energies for all ion species were set at 40 KeV. Implanted films were then analyzed using x-ray photoelectron spectroscopy (XPS). The changes in the chemical composition and bonding chemistry due to ion-implantation were examined at different depths of the films using sequential ion-beam etching and high resolution XPS analysis cycles. A comparative analysis has been made with the results from sputter deposited BCN films suggesting that implanted nitrogen and carbon atoms behaved very similar to nitrogen and carbon atoms in sputter deposited BCN films. We found that implanted nitrogen atoms would prefer bonding to carbon atoms in the films only if there is no boron atom in the vicinity or after all available boron atoms have been saturated with nitrogen. Implanted carbon atoms also preferred to either bond with available boron atoms or, more likely bonded with other implanted carbon atoms. These results were also supported by *ab-initio* density functional theory calculations which indicated that carbon-carbon bonds were energetically preferable to carbon-boron and carbon-nitrogen bonds. © *2011 American Institute of Physics*. [doi:10.1063/1.3638129]

I. INTRODUCTION

Recently, many researchers have been engaged on the synthesis and characterization of solids in the B-C-N ternary system due to their interesting properties, such as extreme hardness and low coefficient of friction.[1–4] B, C, and N are close neighbors in the periodic table with the following electronegativity values; 2.04, 2.55, and 3.04, respectively.[5] However, binary compounds between them exhibit a variety of crystal structures. For example, C exists as graphite and diamond whereas, carbon nitride (C_3N_4) can be synthesized in hexagonal[6] and cubic forms.[7,8] Hexagonal phase of boron nitride (*h*-BN) and graphite share similar layered crystal structures, but the electrical properties for these two are markedly different; *h*-BN is an insulator while graphite is a semimetal.

Most research in the B-C-N ternary are concentrated on single component systems such as diamond like carbon (DLC) films, or two component phases such as BN and C_3N_4, recent studies are motivated by tunable electronic and optical properties of ternary compounds in this system.[9–11] Studies on the boron carbon nitride (BCN) compounds gained much interest after the computational study on the electronic properties of a BCN compound by Liu *et al.*[13] A recent study on the atomic layers of hybridized BN and graphene domains by Ci *et al.*[12] reveals that structural features and bandgap of *h*-BCN are distinct from those of graphene, doped graphene, and *h*-BN. The promising physical properties of BCN materials may potentially allow them to be used in the development of bandgap-engineered applications in electronics and optics,[12,13] as wear-resistant coatings,[14] intercalation material in Li-ion batteries,[15] and low-k dielectric layers in electronics industry.[16]

Various techniques ranging from high temperature/high pressure processing,[17] explosive compaction,[18] pulsed laser deposition,[19] ion-beam assisted deposition,[3,5,20] to magnetron sputtering,[2,21,22] have been used for the synthesis of BCN materials in bulk or as thin films. The physical properties of BCN materials are directly related with the chemical environment, bonding, and atomic structure of the B, C, and N atoms within. Hence, detection and control of the aforementioned during and after the synthesis processes carry utmost importance for the potential technological applications of BCN compounds.

There are several studies which scrutinize the characterization methods used for understanding the atomic environment and bonding structure of BCN films.[2–4,20,23–25] Often, x-ray photoelectron spectroscopy (XPS) has been used for probing the chemical bonding between boron, carbon and nitrogen atoms[2–4,24–28] as binding energy (BE) peak positions in a spectrum obtained during XPS for core shell electrons are affected by the relative electronegativity of coordinated atomic species. While, XPS is a relatively widespread and well-established technique for understanding local chemical interactions in solids, other techniques such

a)Authors to whom correspondence should be addressed. Electronic addresses: bengu@fen.bilkent.edu.tr and nizam3472@yahoo.com.

as electron-energy loss spectroscopy and x-ray absorption near edge spectroscopy have also been used to study the chemistry of BCN systems.[5,20,23,25,27,28] On the other hand, the majority of XPS data presented in the literature for identifying shifts in the BE due to change in local chemistry, are collected from binary compounds or elemental solids. In addition, some of the XPS data for BCN systems show significant scatter as well as overlaps in peak positions.[2,3,22,24,26,28] Furthermore, utilization of peak deconvolution during analysis of XPS spectra often depend on user experience. Hence, these all induce a significant ambiguity in the interpretation of XPS spectra from BCN films.

In order to overcome the issues mentioned above, in this study we have followed a unique procedure to understand the effects of local chemical environment on the B1s, C1s, and N1s regions of the XPS spectra from BCN solids using model systems created by ion implantation. We used r.f. sputter deposition technique to prepare amorphous boron carbide (*a*-BC), amorphous boron nitride (*a*-BN), DLC, and BCN films, which were then ion implanted by C^+, N^+, and N_2^+ ions to synthesize model systems. Then, the XPS data gathered from these model systems were compared to spectra gathered from unimplanted regions of the films and also to spectra acquired from r.f. sputter deposited BCN films. Following these, first-principles plane-wave calculations[29] based on density functional theory (DFT)[30,31] have been performed in order to better understand the changes induced in the bonding behavior by ion implantation. The results are then used to provide more insight into the chemistry of sputter deposited BCN films, also providing a unique opportunity for understanding phase segregation and its effects on BCN solids.

II. EXPERIMENTAL

Thin films of *a*-BC, *a*-BN, and DLC were prepared by r.f. magnetron sputter deposition (RF/MS) on grounded Si (100) substrates using 2 inch targets of B_4C, BN, and carbon (Kurt Lesker, 99.9% purity), respectively. BCN films were also synthesized with the RF/MS technique using a B_4C target on a Si (100) substrate. Prior to the deposition, Si (100) substrates were cleaned for 15 min using r.f. generated Ar plasma. In order to improve the adhesion of the films to the substrate, a Ti buffer layer of approximately 200 nm thick was sputter deposited on the substrates for each film mentioned above. Further detail on the magnetron sputter deposition system used and for the process itself can be found in Ref. 2. The details of the experimental conditions are given in Table I. Implantation experiments were done in a Varian DF4 ion implanter. The details of the experimental conditions are given in Table II.

TABLE I. Experimental conditions for RF/MS deposition where target power, process pressure, and duration were 200 watt, 9×10^{-3} torr and 90 min, respectively.

Target	Process Gas	Substrate Bias	Deposited Films
B_4C	Ar	Grounded	*a*-BC
BN	Ar	Grounded	*a*-BN
Carbon	Ar	Grounded	DLC
B_4C	Ar: N_2	400 V dc bias	BCN

TABLE II. Experimental conditions for implantation experiment where ion energy and dose of the ions were 40 keV and 1.2×10^{18} ion/cm^2, respectively.

Implanted Films	Implanted ion
a-BN	C^+
a-BC	N^+
a-BC	N_2^+
DLC	N^+
DLC	N_2^+

Following the sputter deposition and implantation experiments, chemistry of the films was investigated using XPS with monochromated Al Kα source (Thermo K alpha). The XPS analysis was done ex-situ. The time of elapse between the deposition and the XPS characterization was at most 24 hrs. Resolution of the XPS system was confirmed by measuring the Au 4*f* core line (FWHM $\sim$0.75 eV) by using pass energy of 25 and 0.05 eV step size for data collection. Quantification of the XPS spectra for atomic concentrations was done by normalizing the calculated peak areas using corresponding Scofield factors (0.486 for B1s, 1.0 for C1s, and 1.8 for N1s). For comparison study, BCN films were also deposited on Si (100) substrate using the same procedure mentioned in Table I. The films were found to be amorphous using x-ray diffraction (XRD, Rigaku MiniFlex). Depth profile data were collected using sequential ion beam etching and XPS analysis cycles. First, films were etched by using Ar^+ ion with 3000 eV kinetic energy for 50 s (incident angle; 75° to the normal of the thin film). After etching, XPS data were collected from the etched surface using 200 eV for pass energy and 0.1 eV step size. This procedure was performed several times in a cyclic manner and the data collected were color coded and stacked to form a pseudo-colored image where the X-axis is BE in eV, Y-axis represents the depth from surface in nm. The depth profile images are given as pseudo-color images for B1s, C1s, and N1s. As the signals get stronger for different BE values, hotter pixel colors are assigned to those corresponding BE. Each iso-depth line in these images represents the corresponding XPS spectrum collected at the given depth of the films.

On the other hand, *ab-initio* calculations are carried out by using Vienna *ab-initio* simulation package program.[32–34] The ions are described by the projector-augmented-wave potentials,[35,36] while the plane-wave energy cutoff is set to 500 eV in all calculations for the sake of a high degree of accuracy. Meanwhile, the exchange-correlation potential is expressed in terms of the generalized gradient approximation (Perdew-Wang 91 type[37]). All the systems studied are modeled by large finite sized BN monolayer structures where the edges are saturated by H atoms. Because of the periodic boundary conditions used with plane-wave calculations, a large supercell accommodating the BN nanoribbons with 10 Å of vacuum around it is introduced in order to minimize the ion-ion interaction in the non-periodic directions. Therefore, only the Γ point is enough for the k-point sampling in the Brillouin zone within the Monkhorst-Pack[38] scheme. The

Gaussian smearing, with a smearing parameter of 0.08 eV, is used in consideration of the partial occupancy around the Fermi level. The total energy is converged to within 10^{-5} eV energy threshold in all calculations. The structures are optimized by relaxing the positions of all of the atoms to their minimum energy configurations by using conjugate gradient method where total energy and atomic forces are minimized. Maximum force magnitude remained on each atom is set at most to 0.06 eV/Å.

III. RESULTS AND DISCUSSION

The details of depth profile images with respective spectra for different implanted films at B1s, C1s, and N1s XPS regions are described below separately in Figs. 1–5. The assignments to possible peak position from literatures for different bonding configurations[3,12,19,20,27,39–46] are also shown in those figures. The film thickness, atomic percentage (At%), and ratio of the atoms in ion implanted layers are given in Table III. The depth profiles (range and straggle) for the ions used in the study were calculated for each case using the software for the stopping and range of ions in matter (SRIM) by Ziegler and Biersack[47] and are also included in Table III.

A. C^+ ion implantation into RF/MS deposited *a*-BN boron nitride film

Figure 1(a) shows the XPS generated depth profile images for C^+ ion implanted *a*-BN film for B1s, C1s, and N1s XPS regions and in (b) individual XPS scans for the same regions from ion implanted, unimplanted layers and from a BCN film are provided for comparison. The peak observed in the XPS spectrum for B1s region [dash-dot line line in Fig. 1(b)] of the un-implanted layer suggests two types of B atoms to be present in *a*-BN; first type is indicative of B atoms in B-rich environment like in the elemental B, indicated with B-B in the figure at 188 eV; second type is B atoms in a *h*-BN like nitrogen-rich environment, indicated with B-N at 191 eV.[3,12,19,20] After implantation of the *a*-BN with 40 keV C^+ ions, we found that while the shape of B1s peak indicates a single dominant component [solid black line in Fig. 1(b)] unlike the un-implanted region, it was found to have shifted ~0.5 eV toward lower BE than that for B-N; 190.5 eV. This finding can be interpreted as energetic C^+ ions causing a somewhat homogenization in the bonding behavior of B atoms by forcing an interaction between C and B such as one B surrounded by two N and one C or by two C and one N environment.[3,46] Furthermore, no evidence for the presence of C was observed in the unimplanted layer of the *a*-BN film as expected. The C1s peak in C^+ implanted layer was at a lower binding energy than the C in C environment reported in the literature, 284.2–284.4 eV.[12,19,27,46] This observation also supports the postulate put forth above and indicates that implanted C atoms to be in a B-rich environment. However, we have to emphasize that C environment observed does not exactly match that of C in B_4C, as the peak position is not same as that for B_4C (283.0 eV).[19,40] Two other observations worth mentioning as well; B to C ratio in the implanted region is 2.31 higher than that for B_4C and one can observe a tail at higher binding energy side of the C1s region; solid black line in Fig. 1(b). Thus, some of the implanted C is bonded to B while, the rest is in coordination with other C atoms in the vicinity explaining the C1s

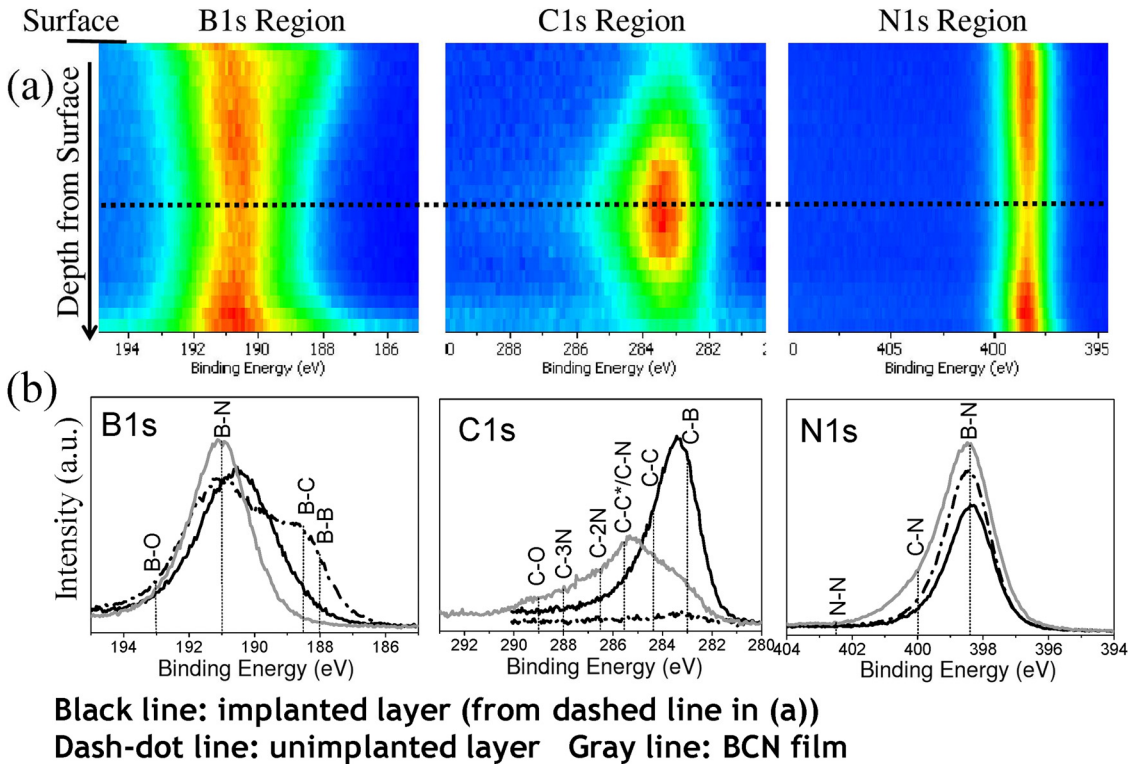

FIG. 1. (Color online) (a) Depth profile images for C^+ ion implanted *a*-BN film at B1s, C1s, and N1s XPS regions, and (b) XPS scans of ion implanted and un-implanted layers from the same sample and BCN films.

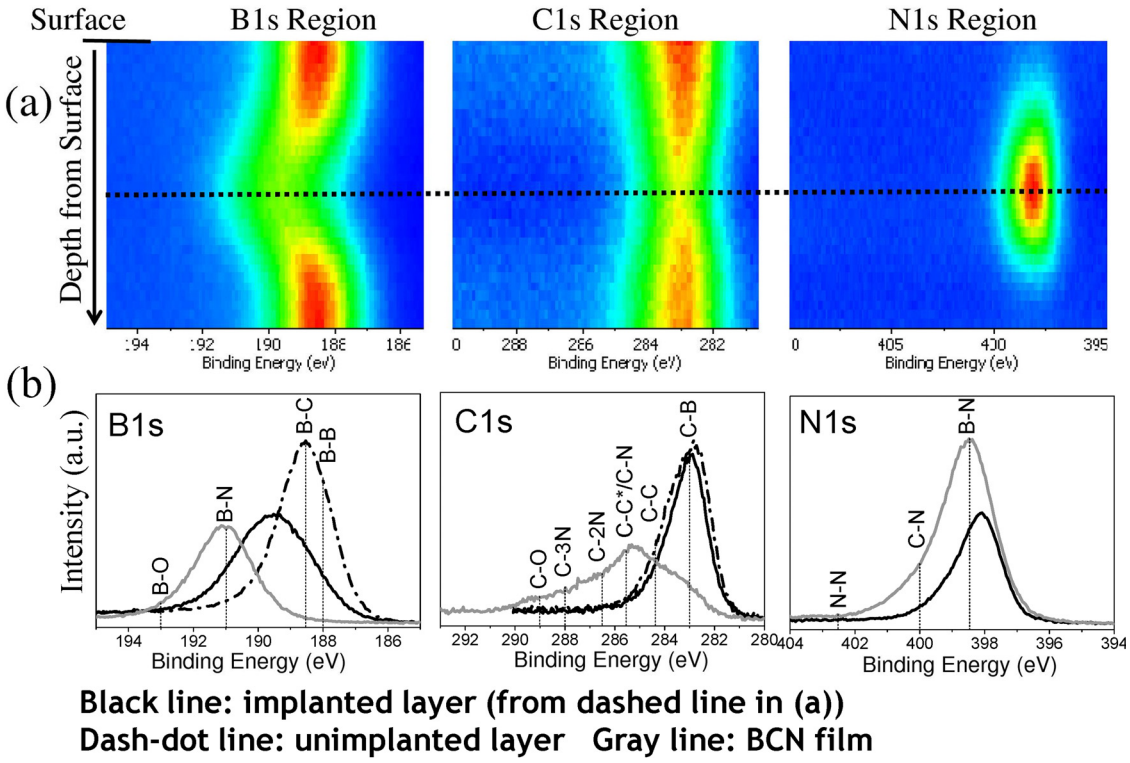

FIG. 2. (Color online) (a) Depth profile images for N^+ ion implanted *a*-BC film at B1s, C1s, and N1s XPS regions, and (b) XPS scans of ion implanted and un-implanted layers from the same sample and BCN films.

peak positioned between C-C and C-B peak positions. Also, from the C1s spectrum, we observed some evidence for C-N coordination at the higher BE tail region. On the other hand, the peak in the C1s spectrum observed for the BCN film (gray line), 285.6 eV, might be a combination of C-N and carbon defect structure (C-C*).[48] Unlike the C1s and B1s spectra, almost no change was observed in the N1s peak position (398.4 eV) after C^+ ion implantation in *a*-BN film. In other words, majority of N atoms were in the BN network before and after C^+ ion implantation.[3,19]

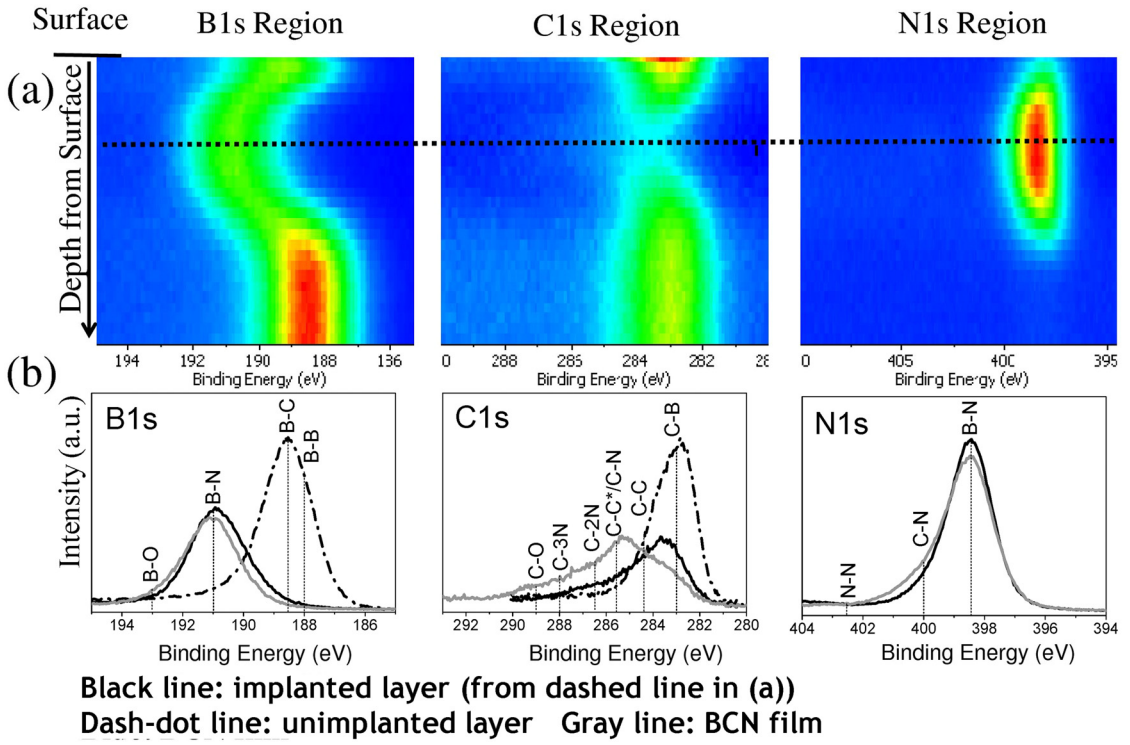

FIG. 3. (Color online) (a) Depth profile images for N_2^+ ion implanted *a*-BC film at B1s, C1s, and N1s XPS regions, and (b) XPS scans of ion implanted and un-implanted layers from the same sample and BCN film.

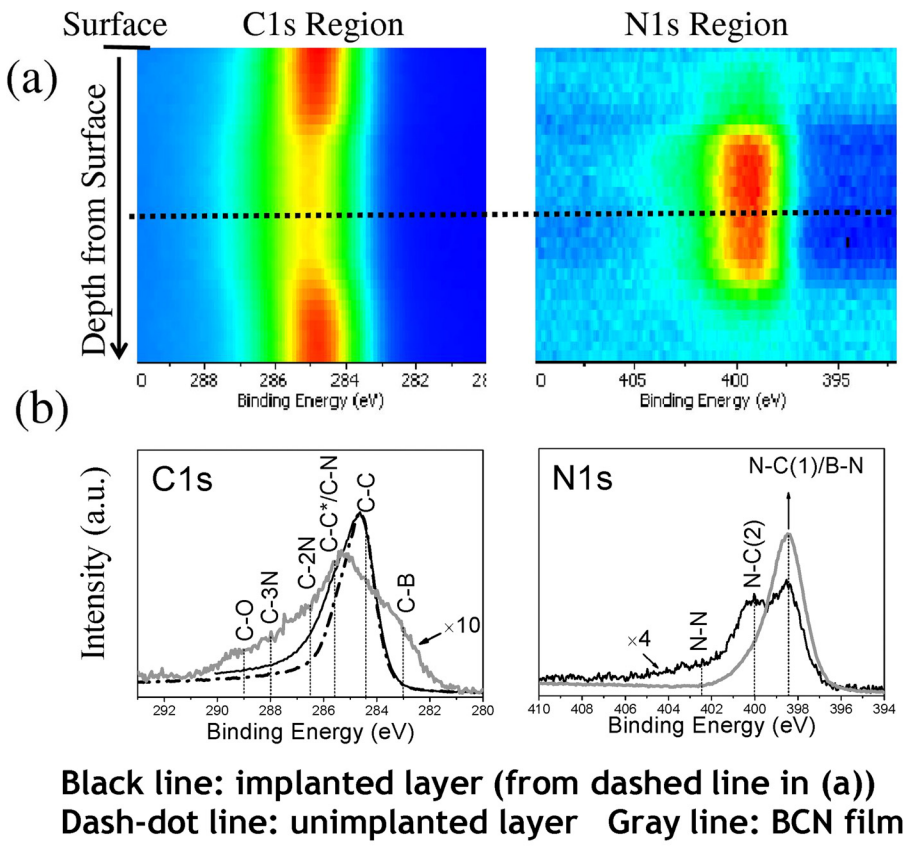

FIG. 4. (Color online) (a) Depth profile images for N^+ ion implanted DLC film at C1s and N1s XPS regions, and (b) XPS scans of ion implanted and un-implanted layers from the same sample and BCN films.

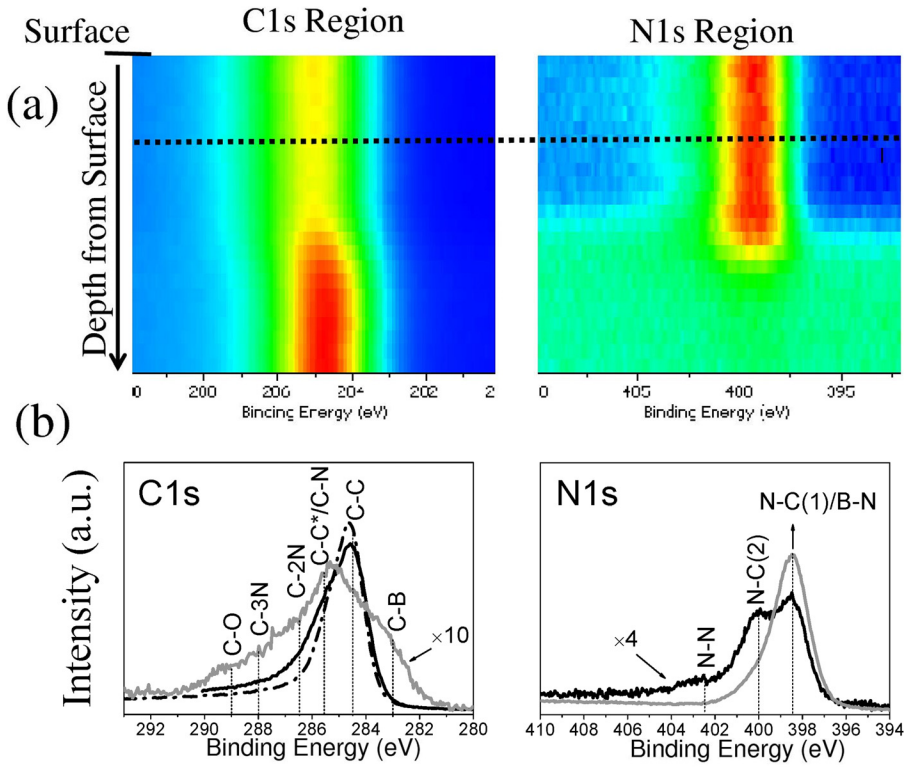

FIG. 5. (Color online) (a) Depth profile images for N_2^+ ion implanted DLC film at C1s and N1s XPS regions, and (b) XPS scans of ion implanted and un-implanted layers from the same sample and BCN films.

TABLE III. Film thickness, atomic percentage, and ratio of the atoms in the implanted layer.

Films	Total thickness (nm)	Depth from the surface[a] (nm)	B	C	N	O	B/N	B/C	SRIM (Å) Range	SRIM (Å) Straggle
C^+ implanted *a*-BN	150	105	47.5	20.5	23.3	8.7	2.04	2.31	959	255
N^+ implanted *a*-BC	210	110	61.5	16.6	19.6	2.3	3.14	3.70	957	241
N_2^+ implanted *a*-BC	210	60	48.5	11.2	38.1	2.2	1.27	4.33	522	159
N^+ implanted DLC	190	75		89.2	9.2	1.6			727	187
N_2^+ implanted DLC	190	40		88.3	9.9	1.8			384	117

[a]The depth from the surface of the film at which the XPS data was obtained and used for chemical composition calculations.

B1s from BCN film [gray line in Fig. 1(b)] shows that B is mostly in BN network with the peak positioned at a slightly higher BE than that of C^+ implanted *a*-BN. B1s spectrum from the BCN films does not indicate a strong presence for B-B bonding in the films. The N1s spectrum from the C^+ implanted film did not reveal an evidence for the presence C-N binding as can be seen in Fig. 1(b). On the other hand, N1s spectrum from the BCN film contains significant evidence for the presence of C-N bonds in addition to B-N bonds. The wide shoulder on the C1s peak for BCN film is also an evidence for the notable C-N contribution in addition to C-C and C-B bonds in the peak shape.

B. N^+ ion implantation into RF/MS deposited *a*-BC film

Figure 2(a) shows the XPS generated depth profile images for N^+ ion implanted *a*-BC film for B1s, C1s, and N1s XPS regions and (b) shows XPS scans of ion implanted and un-implanted layers from the same sample and BCN film. At% and relative ratio of the atoms (Table III) shows that B was dominant the component in the implanted layer. In other words, the matrix was mainly made up of B atoms. Upon N^+ implantation, the B1s peak position has been observed to shift toward higher BE (~189.5 eV) toward B-N position and also the peak was broadened. These suggest energetic N^+ ions causing a change from a B-C dominated bonding configuration toward a new structure where B atoms are likely to be surrounded by more N atoms.[3] The new B1s peak is wide enough to encompass the environments of B-N (191 eV), B-B (188 eV), and B-C (188.5 eV).[3,12,19,20] On the other hand, almost no change has been observed in the C1s peak position and shape after implantation. This observation may suggest that the C atoms were still in a B-C dominated environment with perhaps a small contribution from C-C bonds, but no C-N contribution was observed. Whereas, C1s from BCN film [Fig. 2(b)] shows that C is mostly in C-C network with significant contribution of C-B and C-N structures. N1s peak position with the center of 398 eV implies that N in the implanted layer was mostly in BN network.[12,41]

C. N_2^+ ion implantation into RF/MS deposited *a*-BC film

Figure 3(a) shows the XPS generated depth profile images for N_2^+ ion implanted *a*-BC film for B1s, C1s, and N1s XPS regions and (b) shows XPS scans of ion implanted and un-implanted layers from the same sample and BCN film. At% and relative ratio of the atoms (Table III) shows that B and N were high in the implanted layer compared to C. In this case, the number of implanted ion was same as in the N^+ ion implanted film but the number of N atom was twice than that in N^+ ion implanted film. A strong shift in B1s peak position to higher BE at around 191 eV for N_2^+ implanted region was observed. This indicates that the B atoms are in a *h*-BN like environment. Implantation of N_2^+ ions also affected the C1s peak shape and position. A shoulder becomes apparent in the higher BE part of the C1s peak and the peak is shifted to higher BE. It is rather clear that N_2^+ implantation caused a notable change in the bonding of boron which preferred bonding to highly electronegative and energetic N atoms. In the C1s region after implantation, several different possible C-N bonding combinations are observed at peak positions around 285.6, 284.4, and 283 eV.[12,27,29,40] The C-B bond is also seen in the C1s region but that contribution is not so obvious in the B1s region. This might be due to the amount of B which is four times higher than that of C in the implanted regions. N1s peak position with the peak center at 398.4 eV implies that N in the implanted layer was mainly in BN network.[1,3] While we observed a strong indication of C-N bond in the C1s region, the evidence of C-N bonding in the N1s spectrum from the implanted region is not very clear. This could be explained by the presence of an extremely N rich environment in the implanted region, as shown in Table III. Hence, even if some C is bonded to N atoms, the effect would be more prominent in the C1s region as majority of the N is coordinated to B and so the fraction of N atoms bonded to C would be very little. Furthermore, in some studies the peak at around 398.4 eV is also reported for sp^2C-N.[42,43]

D. N^+ and N_2^+ ion implantation into RF/MS deposited DLC films

Figures 4(a) and 5(a) show the XPS generated depth profile images for N^+ and N_2^+ ions implanted DLC films at C1s and N1s XPS regions, respectively, and (b) of those show XPS scans of ion implanted and un-implanted layers from the same sample and BCN film. In these cases, the total number of implanted ions was the same but the number of N atoms were twice as high for N_2^+ implanted film. The shape and peak position of C1s peak are same for both implantation

cases as shown in (b) of Figs. 4 and 5. But the shape of C1s peak for implanted layer was different than that for unimplanted layer of C film. There is a slight shoulder at higher BE of C1s which may imply some bonding of C with N. The possible peaks in C1s could be assigned to C in C environment at 284.4 eV, C bonded with one N at 285.6 eV, and C bonded with two N at 286.5 eV.[12,19,27,40] N1s peaks for both cases seem to be combination of three bonding structures. The possible peaks could be assigned to N atoms having two C neighbors at 398.4 eV [N-C(1)], N atoms having three C neighbors at 400.0 eV [N-C(2)][42–45] and N bonded with other N atoms or suggest some trapped N_2 at 402.5 eV.[43] It is very clear from Figs. 5 and 6 that N prefer to make bond with C in absence of B.

Figure 6 compares the B1s, C1s, and N1s data from different implanted films directly. It shows that addition of small amount of nitrogen (N^+) first affected the B atom only. With further increase of the amount of implanted nitrogen ($N^+ \rightarrow N_2^+$), a shift to higher BE has been observed for C1s peak in addition to that of B1s peak. A shoulder became apparent at higher binding energy of C1s peak which indicates the formation of C-N bonds. Thus implanted nitrogen into sputter deposited boron carbide prefers firstly B atom. The excess N atoms then started to bind with C after B was saturated with implanted N. Figure 6 also indicates that the implanted C^+ ion did not affect N peak position and shape. These indicate that neither C nor N atoms prefer each other to make bond if there are B atoms around.

In order to get clearer pictures of bonding behavior between B, C, and N, we deposited BCN thin films at different N_2 fluences. Figure 7 shows the XPS spectra of BCN for (a) B1s, (b) N1s, and (c) C1s regions from the films deposited at increasing N_2 fluences. B1s and C1s spectra from B_4C target are also shown here for the comparison. Figure 7(a) shows that peak position for B-C bonding in the B1s spectra shifts toward that of B-N with the increase of N_2 fluence. The B-C bonding contribution is almost negligible for the films deposited using 5 to 10% N_2 in the process gas. No significant peak of N-C bonding could be seen for the films deposited using N_2 fluence up to 3% [Fig. 7(b)]. A shoulder, possibly due to N-C bonding, become apparent at higher BE of N1s (400–402 eV) for the films deposited with 5 to 10% N_2 fluence. This shoulder becomes more prominent with the increase of N_2 fluence. This may imply that N started to bond with C when B reached saturation at around 3% N_2 fluence in our case. On the other hand, Fig. 7(c) shows that intensity of the peaks assigned for C-B bonding decreases with the increase of N_2 fluence. Some shoulders could be seen at higher BE region (287–290 eV), especially for the film deposited using 5% to 10% N_2 fluence. Those peaks are assigned to C bonded to N with different ratios. The most intense peak (285.4 eV) that observed at highest fluence of N_2 is assigned to $sp^2C=N$.[2,19,27,49]

We have also investigated the carbon incorporation to the boron nitride monolayer by total energy calculations which have been performed for various structures, especially the carbon substitution, by using DFT. Those structures are compared in terms of defect energy which is defined with respect to the perfect BN nanoribbons as follows:

$$E_{def}[\mathrm{BN}+\mathrm{C}] = E_{tot}[\mathrm{BN}-\mathrm{C}] - E_{tot}[\mathrm{BN}] - n_C\mu_C + n_B\mu_B + n_N\mu_N, \quad (1)$$

where E_{tot}[BN-C] is the total energy of C implanted BN (BN-C) structure, E_{tot}[BN] is the total energy of planar BN structure without carbon impurity and n's are the difference in the number of atoms with respect to the perfect BN films for each species and μ_C, μ_B, and μ_N are the chemical potentials of carbon, boron, and nitrogen, respectively. Hence, the total chemical potential of incorporated carbon atoms is subtracted and total chemical potentials of missing boron and nitrogen atoms with respect to the reference (perfect BN structures) are added with this definition of E_{def}. Alpha-boron, graphite, and gas phase structures for boron, carbon, and nitrogen, respectively, have been used in order to calculate the corresponding chemical potentials. The results are summarized in Table IV. For single carbon substitution the foreign carbon atom is replaced at boron site and nitrogen

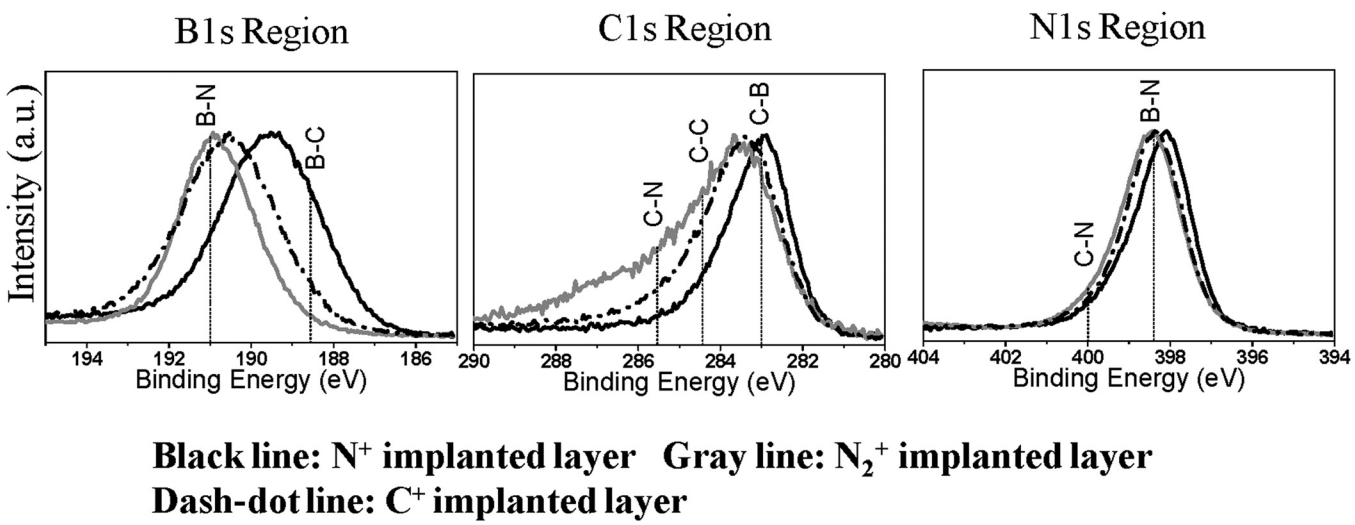

FIG. 6. Comparison of normalized XPS data obtained from ion implanted layer; dash-dot line for C^+ implanted *a*-BN film, black line for N^+ implanted *a*-BC film, gray for N_2^+ implanted *a*-BC film.

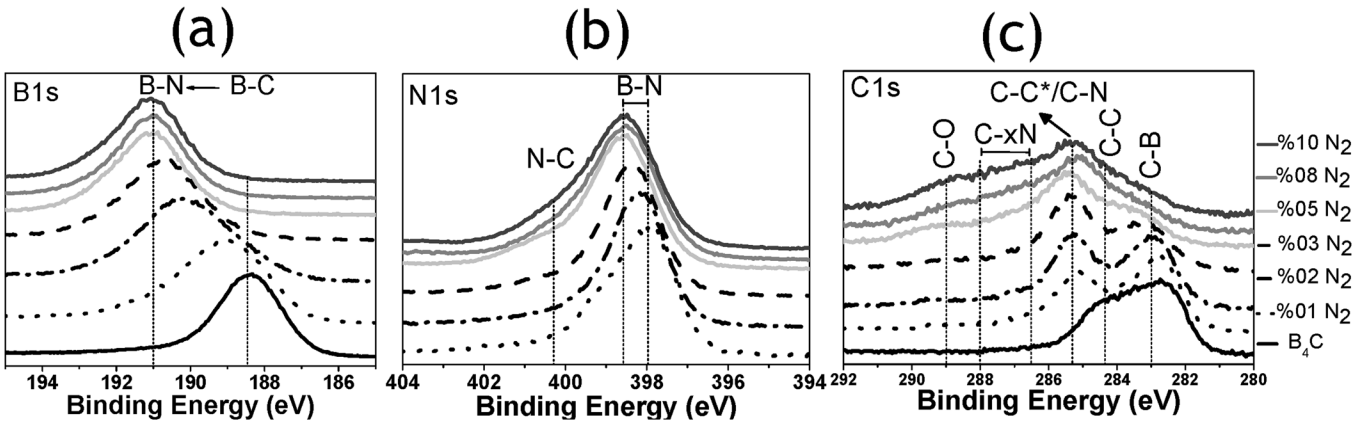

FIG. 7. XPS spectra for (a) B1s, (b) N1s, and (c) C1s regions from the films deposited at increasing N_2 fluences. B1s and C1s spectra from B_4C target are also shown here for the comparison.

site, respectively, as shown in Fig. 8. The defect energies are 4.27 eV for N site and 4.38 eV for B site, which suggest that carbon atom initially prefers to form C-B bonds by replacing nitrogen. Figure 9 shows the structures for the cases of two carbon substitution where (a) shows the formation of C-C pair and (b) shows the distance between two carbons; 2.904 Å. Figures 9(a) and 9(b) represent the substitutions for both N and B sites. Defect energy for pair case is the lowest (4.68 eV) among other 2C substitutions. It implies that the structure with C-C pair substitution is energetically favorable than those of others. Thus, carbon atoms prefer to make C-C bonds and tend to congregate in BN monolayer. Figures 9(c) and 9(d) refer to structures for 2C substitution in only boron sites and only nitrogen sites, respectively. We repeated same calculations for various C-C distances and the defect energies are found to be around 8.4–8.5 eV. This result is in good agreement with the case of one C substitution where the defect energies will be approximately half. Thus the structures behave like two separate defects. It is also implied that the defect energy reduces with the increasing number of C-C bonds.

The electronic structure and the charge density are important to understand the details of experiments like XPS. Therefore, we have presented the charge density differences with respect to BN layer of single carbon substitution on BN

TABLE IV. Defect energies for single and double carbon substitution into BN layer. Number of bonds and magnetic moments are shown. The structures are shown in Figs. 8 and 9. The defect energies have been calculated using Eq. (1).

Structure	Number of C-C bonds	Number of C-B bonds	Number of C-N bonds	Magnetic moment (μ_B)	E_{def} (eV)
C in B site	0	0	3	1.0	4.38
C in N site	0	3	0	1.0	4.27
C-C pair	1	2	2	~0	4.68
2C in both B & N sites apart	0	3	3	~0	6.49
2C in 2B sites	0	0	6	~0	8.49
2C in 2N sites	0	6	0	~0	8.39

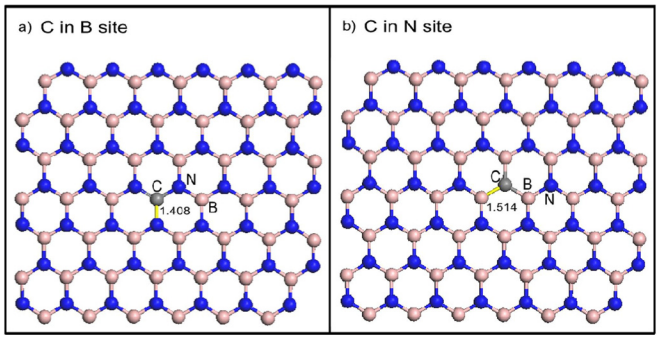

FIG. 8. (Color online) Single carbon atom substitution on (a) B site and (b) N site. The bond lengths are indicated in the figure. Calculations are performed by starting planar and nonplanar geometries. The planar final geometry is energetically most favorable.

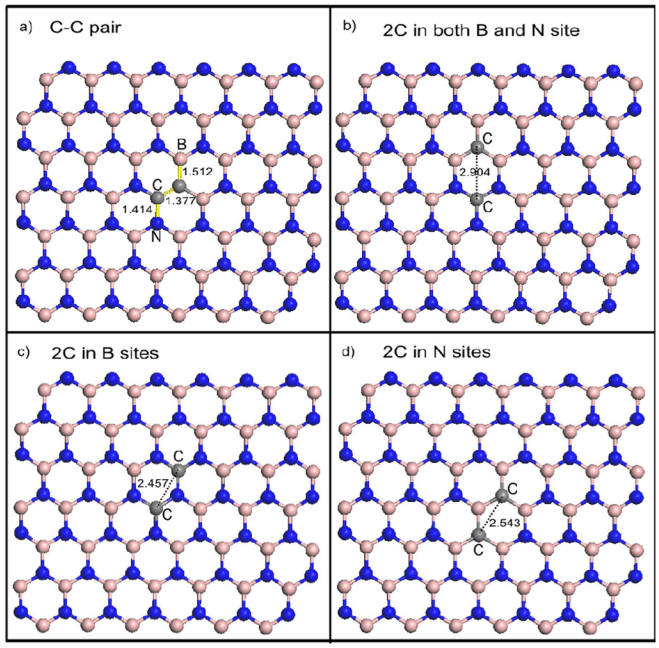

FIG. 9. (Color online) Double carbon substitution into BN layer; (a) carbon atoms make C-C pair, (b) B and N are replaced by carbons with distance 2.904 Å, (c) two boron atoms are replaced by carbons, (d) two nitrogen atoms are replaced by carbons. The defect energies are given in Table IV. The C-C pair has the lowest defect energy (4.68 eV).

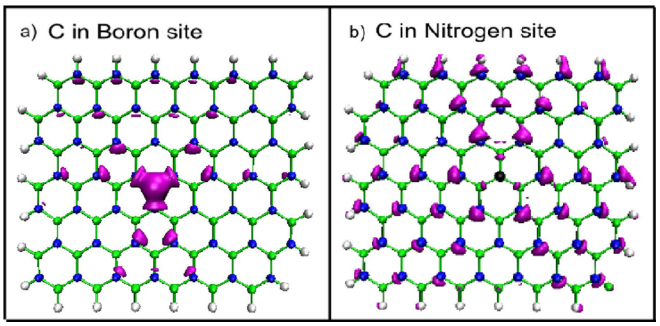

FIG. 10. (Color online) Difference charge density plots with respect to BN layer for single carbon substitution to (a) boron site, (b) nitrogen site. Since in BN layer the charges are congregate in N sites, we have excess charge on carbon for boron replacement.

structures in Fig. 10. The reference structure is the BN layer. The charges are congregate on nitrogen sites in the reference structure. Boron, carbon, and nitrogen have 3, 4, and 5 valance electrons, respectively. Hence, for carbon substitution into boron site the excess charge remains on carbon. In the case of C atom in a Boron site, the charge due to the extra electron from substitutional carbon atom is distributed locally. Whereas, the extra charge due to a carbon atom exchanging a nitrogen atom in the system were found to be distributed in an extensive manner; effects reaching as far as the boundaries of the BN layer used for the computational studies. Surely, this point requires further study, and could be used to provide valuable insights to understanding the chemistry of B-C-N solids and alike through XPS and related techniques.

IV. CONCLUSIONS

A comparative study in terms of experimental and DFT investigation was performed to understand the individual effect of atoms in the bonding structures and the possible phase separation routes in BCN materials. In that concern, N^+ and N_2^+ ions were implanted into RF/MS deposited DLC and *a*-BC films, and C^+ ions were implanted into RF/MS deposited *a*-BN films. In addition, BCN films were sputter deposited using different N_2 fluences. The results were explained using depth profile images with respective spectra for different films at B1s, C1s, and N1s XPS regions. The results revealed that N and C do not prefer to bond with each other if there are B atoms in the vicinity. At high N_2 fluence (5%–10%) in BCN film deposition or N_2^+ ion implantation, N bonded to C after the bonding saturation of B-N structure. In addition, implanted C atoms also preferred to either bond with boron atoms which were not coordinated with nitrogen atoms, or bonded with other carbon atoms. DFT investigation also supported these experimental findings. These results could be used as important references for future works in the related fields.

ACKNOWLEDGMENTS

The authors would like to acknowledge financial support for the work by TUBITAK (Grant No. 106T328 and 107T892) and European Union 7. Framework project Unam-Regpot (Grant No. 203953). Author Md. Nizam Uddin would like to thank Shahjalal University of Science and Technology, Bangladesh for the permission of leave.

[1]V. L. Solozhenko and E. Gregoryanz, Mater. Today **8**, 44 (2005).
[2]E. Bengu, M. F. Genisel, O. Gulseren, and R. Ovali, Thin Solid Films **518**, 1459 (2009).
[3]M. N. Uddin, I. Shimoyama, Y. Baba, T. Sekiguchi, and M. Nagano, J. Vac. Sci. Technol. **A23**, 497 (2005).
[4]M. N. Uddin, I. Shimoyama, Y. Baba, T. Sekiguchi, K. G. Nath, and M. Nagano, Appl. Surf. Sci., **241**, 246 (2005).
[5]R. Gago, I. Jimenez, J. M. Albella, and L. J. Terminello, Appl. Phys. Lett. **78**(22), 3430 (2001).
[6]P. V. Zinin, L.-C. Ming, S. K. Sharma, V. N. Khabashesku, X. Liu, S. Hong, S. Endo, and T. Acosta, Chem. Phys. Lett. **472**, 69 (2009).
[7]Y. J. Tian, D. L. Yu, J. L. He, F. R. Xiao, T. S. Wang, D. C. Li, L. Li, G. Zheng, and O. Yanagisawa, J. Cryst. Growth **225**, 67 (2001).
[8]T. S. Wang, D. L. Yu, Y. J. Tian, F. R. Xiao, J. L. He, D. C. Li, W. K. Wang, and L. Li, Chem. Phys. Lett. **334**, 7 (2001).
[9]S. Kumar, N. Kamaraju, K. S. Vasu, A. Nag, A. K. Sood, and C. N. R. Rao, Chem. Phys. Lett. **499**, 152 (2010).
[10]J. Yang, T. Qiu, and C. Y. Shen, Chin. Phys. Lett. **23**(9), 2573 (2006).
[11]X. D. Bai, E. G. Wang, J. Yu, and H. Yang, Appl. Phys. Lett. **77**(1), 67 (2000).
[12]L. Ci, L. Song, C. Jin, D. Jariwala, D. Wu, Y. Li, A. Srivastava, Z. F. Wang, K. Storr, L. Balicas, F. Liu, and P. M. Ajayan, Nature Mater. **9**, 430 (2010).
[13]A. Y. Liu, R. M. Wentzcovitch, and M. L. Cohen, Phys. Rev. B **39**, 1760 (1989).
[14]V. L. Solozhenko, D. Andrault, G. Fiquet, M. Mezouar, and D. C. Rubie, Appl. Phys. Lett. **78**, 1385 (2001).
[15]M. Morita, T. Hanada, H. Tsutsumi, Y. Matsuda, and M. Kawaguchi, J. Electrochem. Soc. **139** (5), 1227 (1992).
[16]Y. Etou, T. Tai, T. Sugiyama, and T. Sugino, Diamond Relat. Mater. **11**, 985 (2002).
[17]S. Nakano, M. Akaishi, T. Sasaki, and S. Yamaoka, Chem. Mater. **6**, 2246 (1994).
[18]Y. Zhao, D. W. He, L. L. Daemen, T. D. Shen, R. B. Schwarz, Y. Zhu, D. L. Bish, J. Huang, J. Zhang, G. Shen, J. Qian, and T. W. Zerda, J. Mater. Res. **17**, 3139 (2002).
[19]H. Ling, J. D. Wu, J. Sun, W. Shi, Z. F. Ying, and F. M. Li, Diamond Relat. Mater. **11**, 1623 (2002).
[20]M. N. Uddin, I. Shimoyama, Y. Baba, T. Sekiguchi, K. G. Nath, and M. Nagano, J. Appl. Phys. **99**, 084902-1 (2006).
[21]V. Linss, S. E. Rodil, P. Reinke, M. G. Garnier, P. Oelhafen, U. Kreissig, and F. Richter, Thin Solid Films **467**, 76 (2004).
[22]S. Nakao, T. Sonoda, K. Tsugawa, J. Choi, and T. Kato, Vacuum **84**, 642 (2010).
[23]R. Gago, I. Jimenez, U. Kreissig, and J. M. Albella, Diamond Relat. Mater. **11**, 1295 (2001).
[24]S. Chattopadhyay, L. C. Chen, S. C. Chien, S. T. Lin, and K. H. Chen, J. Appl. Phys. **92**(9), 5150 (2002).
[25]S. C. Ray, H. M. Tsai, C. W. Bao, J. W. Chiou, J. C. Jan, K. P. Krishna Kumar, W. F. Ponga, M.-H. Tsai, S. Chattopadhyay, L. C. Chen, S. C. Chien, M. T. Lee, S. T. Lin, and K. H. Chen, J. Appl. Phys. **96**(1), 208 (2004).
[26]C. Zhuang, J. Zhao, F. Jia, C. Guan, Z. Wu, Y. Bai, and X. Jiang, Surf. Coat. Technol. **204**, 713 (2009).
[27]M. A. Mannan, Y. Baba, T. Kida, M. Nagano, I. Shimoyama, N. Hirao, and H. Noguchi, Thin Solid Films **519**, 1780 (2010).
[28]M. A. Mannan, H. Noguchi, T. Kida, M. Nagano, N. Hirao, and Y. Baba, Thin Solid Films **518**, 4163 (2010).
[29]M. C. Payne, M. P. Teter, D. C. Allan, T. A. Arias, and J. D. Joannapoulos, Rev. Mod. Phys. **64**, 1045 (1992).
[30]P. Hohenberg and W. Kohn, Phys. Rev. **136**, B864 (1964).
[31]W. Kohn and L. J. Sham, Phys. Rev. **140**, A1133 (1965).
[32]G. Kresse and J. Hafner, Phys. Rev. B **48**, 13115 (1993).
[33]G. Kresse and J. Furthmüller, Comput. Mater. Sci. **6**, 15 (1996).
[34]G. Kresse and J. Furthmüller, Phys. Rev. B **54**, 11169 (1996).
[35]P. E. Blöchl, Phys. Rev. B **50**, 17953 (1994).
[36]G. Kresse and D. Joubert, Phys. Rev. B **59**, 1758 (1999).
[37]J. P. Perdew, J. A. Chevary, S. H. Vosko, K. A. Jackson, M. R. Pederson, D. J. Singh, and C. Fiolhais, Phys. Rev. B **46**, 6671 (1992).
[38]H. J. Monkhorst and J. D. Pack, Phys. Rev. B **13**, 5188 (1976).
[39]T. Hasegawa, K. Yamamoto, and Y. Kakudate, Diamond Relat. Mater. **11**, 1290 (2002).

[40]M. O. Watanabe, T. Sasaki, S. Itoh, and K. Mizushima, Thin Solid Films **281–282**, 334 (1996).
[41]I. Shimoyama, Y. Baba, S. Tetsuhiro, K. G. Nath, M. Sasaki, and K. Okuno, J. Vac. Sci. Technol. A **21**(6), 1843 (2003).
[42]X. Li, J. Zhang, L. Shen, Y. Ma, W. Lei, Q. Cui, and G. Zou, Appl. Phys. A **94**, 387 (2009).
[43]P. Hammer and F. Alvarez, Thin Solid Films **398–399**, 116 (2001).
[44]J. Zhang, W. Liu, X. Li, B. Zhan, Q. Cui, and G. Zou, Mater. Res. Bull. **44**, 294 (2009).
[45]C. Ronning, H. Feldermann, R. Merk, H. Hofsass, P. Reinke, and J.-U. Thiele, Phys. Rev. B **58**(4), 2207 (1998).
[46]R. Soufli, A. L. Aquila, F. Salmassi, M. F. Perea, and E. M. Gullikson, Appl. Opt. **47**(25), 4633 (2008) and references therein.
[47] J. F. Ziegler, J. P. Biersack, and U. Littmark, *The Stopping and Ranges of Ions in Solids* (Pergamon Press, New York, 1985).
[48]H. E. Szwarckopf, Carbon **42**, 1713 (2004).
[49]Y. M. Chen, Z. X. Zeng, S. R. Yang, and J. Y. Zhang, Diamond Rel. Mater. **18**, 20 (2009).